Available online at www.sciencedirect.com
SCIENCE DIRECT
Catalysis Today 114 (2006) 31–39
CATALYSIS TODAY
www.elsevier.com/locate/cattod

La–Li–Cr perovskite catalysts for diesel particulate combustion

Debora Fino *, Nunzio Russo, Emanuele Cauda, Guido Saracco, Vito Specchia

Materials Science and Chemical Engineering Department, Politecnico di Torino, Corso Duca degli Abruzzi 24, 10129 Torino, Italy

Available online 22 March 2006

Abstract

Nano-structured bulk Li-substituted La–Cr perovskites ($La_{0.8}Cr_{0.9}Li_{0.1}O_3$, $La_{0.8}Cr_{0.8}Li_{0.2}O_3$, $La_{0.8}Cr_{0.7}Li_{0.3}O_3$) were prepared (by combustion synthesis), characterized (by XRD, AAS, BET, SEM, TEM, TPD/R, XPS analyses), tested (in a temperature-programmed combustion TPC microreactor and in a DSC analyzer) in comparison with the reference $LaCrO_3$. The progressive increase in the Li content of the catalysts induces an increase in the catalytic activity owing to the enhancement of the amount of weakly chemisorbed oxygen O^- species (even exceeding 1200 μmol/g), key players in the soot oxidation mechanism. However, beyond 20% Cr substitution with Li, part of this latter metal got segregated as $LiCrO_2$. The best single-phase catalyst ($La_{0.8}Cr_{0.8}Li_{0.2}O_3$) was already active well below 350 °C. Catalytic traps were prepared by in situ combustion synthesis within cordierite (CORNING) and SiC (IBIDEN) wall-flow filters on the basis of the above catalysts and tested on real diesel exhaust gases in an engine bench, fully confirming the encouraging results obtained on powder catalysts.

Keywords: Li-substituted La chromites; Catalytic combustion; Diesel particulate; Soot; Suprafacial oxygen; Wall-flow trap

1. Introduction

The exhaust gases of diesel engines are known to be a hazard to human health. In this context, particulate raises a special concern, due to its carcinogenic effect [1], which has stimulated the development of emission reduction technologies. Not withstanding the efforts to improve the fuel injector design in the last decade, soot emissions could not be reduced down to values lower than the limits of the pending EURO IV legislation (to be enforced in 2005). A promising alternative is the development of a multifunctional catalytic filter that combines filtration and oxidation of the emitted particulate matter. In this context, the key is to find a catalyst that decreases the combustion temperature of soot as much as possible so as to limit the energy requirements of periodic trap heating for regeneration purposes. Catalytic traps based on wall-flow ceramic monoliths (shallow-bed filtration), combined with an oxidation catalyst deposited onto their inlet channel walls, are being developed and tested worldwide [2–8]. These traps can be periodically regenerated by a peculiar use of last generation Common-Rail Diesel engines: some fuel is post-injected and gets burned out by a specific catalytic converter so as to heat up the exhaust gases entering the downstream trap until catalytic combustion of soot is ignited. In an earlier paper alkali-substituted $LaCrO_3$ perovskite catalysts [9] were shown to have promise for this application. In particular, La substoichiometry and the addition of Li at the Cr site were found to lead to a very active catalyst: $La_{0.8}Cr_{0.9}Li_{0.1}O_3$. On the grounds of these promising results, this paper describes the further developments undertaken for the sake of fully assessing the potential of lithium-substituted lathanum chromites. The role of the various constiuting elements is assessed as well as the key steps of the soot combustion mechanism. Finally, the perfomance of wall-flow traps lined with the mentioned catalysts is checked and discussed at an engine bench level.

2. Materials and methods

2.1. Catalyst preparation

The following perovskite catalysts were prepared: $LaCrO_3$, $La_{0.8}Cr_{0.9}Li_{0.1}O_3$, $La_{0.8}Cr_{0.8}Li_{0.2}O_3$, $La_{0.8}Cr_{0.7}Li_{0.3}O_3$. The rationale of this selection was the introduction of an as large as possible amount of Li at the chromium site of La-substoichiometric perovskites. La substoichiometry was indeed found to pay off in terms of catalytic activity, as discussed in [9]; it was maximized in all perovskite samples containing Li.

* Corresponding author. Tel.: +39 011 5644710; fax: +39 011 5644699.
E-mail address: debora.fino@polito.it (D. Fino).

0920-5861/$ – see front matter © 2006 Elsevier B.V. All rights reserved.
doi:10.1016/j.cattod.2006.02.007

Higher La deficiencies compared to $LaCrO_3$ stoichiometry cannot be hosted in the perovskite structure.

The preparation method employed was the so-called "*combustion synthesis*", based on a highly exothermic and self-sustaining reaction [10]. This technique is particularly suited to produce nanosized catalyst particles. A nano-structured and foamy catalyst coating over the diesel particulate trap could effectively improve the local catalyst-soot contact conditions, a critical issue in this field [2].

Taking as a reference the preparation of $LaCrO_3$, the synthesis route can be formally split into two steps:

$$2La(NO_3)_3 + 2Cr(NO_3)_3 \rightarrow 2LaCrO_3 + 6N_2 + 15O_2 \quad (1)$$

$$10CO(NH_2)_2 + 15O_2 \rightarrow 10CO_2 + 20H_2O + 10N_2 \quad (2)$$

This is a very simplified view of a much more complex process which is far from being completely understood (see [10] for deeper details). Reaction (1) is endothermic and represents the perovskite synthesis starting from the metal nitrate precursors (Fluka), whereas Reaction (2) is exothermic and accounts for the reaction between the oxygen derived from nitrates decomposition and urea. Some direct urea decomposition and combustion with atmospheric oxygen forced us to adopt a 250% excess of urea compared to the stoichiometry of the above set of reactions. The synthesis is in fact carried out in air within an electric oven kept at 600 °C which hosts the precursors mixture located in a porcelain vessel in batches leading to the production of a couple of grams per run. The overall exothermic nature of the reactions leads to a thermal peak well exceeding 1000 °C for a few seconds in the reacting solid mixture. To even emphasize this sudden heat release, some NH_4NO_3 was added to the precursor mixture (1 g of NH_4NO_3 per perovskite gram), as suggested in [10]. Under these conditions, nucleation of nanosized perovskite crystals is induced, their growth being limited.

All catalysts were then ground in a ball mill at room temperature prior to characterization.

2.2. Catalyst characterization

Compositional analysis (dissolution in HNO_3/HCl followed by atomic absorption analysis with a Perkin-Elmer 1100B spectrometer) was performed on all prepared samples to confirm that the expected elements were present in the prepared catalysts in the due amounts.

X-ray diffraction (PW1710 Philips diffractometer equipped with a monochromator for the Cu Kα radiation) was adopted on all fresh catalysts to examine whether the desired perovskite structure was actually achieved.

BET specific surface areas of the prepared catalysts were evaluated by use of a Micromeritics ASAP 2010 analyzer.

Direct observation of the nanosized perovskite crystals was performed by transmission electron microscopy (TEM – Philips CM 30 T), whereas Field Emission Scanning Electron Microscope (FESEM – Leo 50/50 VP with GEMINI column) was employed to analyze the microstructure of the catalyst layer deposited over the SiC and cordierite traps according to the procedures described in Section 2.4.

X-ray photoelectron spectroscopy was used to characterize the surface composition of the basic $LaCrO_3$, the $La_{0.8}Cr_{0.9}Li_{0.1}O_3$, and the $La_{0.8}Cr_{0.8}Li_{0.2}O_3$ perovskites, by means of a VG Escalab 200-C X-ray photoelectron spectrometer using a non-monochromatic Mg Kα source. A 20 eV pass energy, resolution of 1.1 eV and a step of 0.2 eV were used for high resolution spectra. The effects of sample charging were eliminated by referring the spectral lines shift to the C 1s binding energy value of 284.6 eV. Quantitative analysis of the catalyst surface composition was determined by integration of the areas below the XPS peaks with the software ECLIPSE v3.1 VG Scientific using the peak-fitting techniques for the Cr $2p_{3/2}$, La $3d_{5/2}$ and O 1s regions; peaks areas were then normalized taking into account the Shirley background [11] and the Scofield [12] sensibility factors. The XPS measurements were performed on the catalysts after two different thermal treatments: 60 min at 600 °C in pure oxygen with a pressure value of 1.1 bar (simulating oxidizing conditions) and 2 h at 400 °C in Ultra High Vacuum ($<2 \times 10^{-9}$ mbar; simulating reducing conditions).

Some temperature-programmed analyses were performed in a Thermoquest TPD/R/O 1100 analyzer, equipped with a thermal conductibility (TCD) detector. A fixed bed of catalyst was enclosed in a quartz tube and sandwiched between two quartz-wool layers; prior to each temperature-programmed oxygen desorption (TPD) run, the catalyst was heated under an O_2 flow (40 Nml/min) up to 750 °C. After 30 min stay at this temperature as a common pre-treatment, the temperature was lowered down to 25 °C under the same flow rate of oxygen, thereby achieving complete saturation. Afterwards, He was fed to the reactor at a 10 ml/min flow rate and kept up for 1 h at room temperature in order to purge out any excess oxygen. The catalyst was then heated up to 1100 °C at the constant heating rate of 10 °C/min under the same helium flow rate. The total amount of O_2 desorbed during the heating protocol was detected by the TCD detector after proper calibration. Temperature-programmed reduction (TPR) experiments were carried out in the same apparatus. After the same oxidation pre-treatment adopted for the TPD runs, the sample was reduced with a 4.95% H_2/Ar mixture (10 Nml/min) meanwhile heating at a 10 °C/min rate up to 1100 °C. Once again, via the TCD detector the amount of the H_2 converted could be monitored.

2.3. Catalytic activity test and apparent activation energy determination

The catalytic activity of the prepared catalysts was tested in a temperature-programmed combustion (TPC) apparatus. A detailed description of the TPC equipment has been reported in [13]. This equipment mainly consists of a fixed bed inserted in a quartz microreactor (i.d.: 4 mm). The fixed bed was prepared by mixing 50 mg of a 1:9-by-weight mixture of carbon and powdered catalyst with 150 mg of silica pellets (0.3–0.7 mm in size); this inert material was adopted to reduce the specific

pressure drop across the reactor and to hinder thermal runaways. Amorphous carbon particles by Cabot Ltd. were used for the sample preparation (about 45 nm in diameter; BET specific surface area = 200 m^2/g; 0.34% of ashes after calcination at 800 °C; 12.2% of adsorbed water moisture; no adsorbed hydrocarbons and sulfates). This type of carbon was used because it burns at temperatures close to those typical of real diesel particulate without bearing any volatile hydrocarbon fraction. The catalyst–carbon mixture was obtained by careful grinding in an agate mortar. This corresponds to contact conditions generally referred to as "tight" [2], which are too intensive compared to what is actually achievable in a catalytic soot trap. Tight contact entails a much higher degree of reproducibility which sets a good basis for activity screening studies and activation energy measurements.

The catalyst/carbon/SiO_2 mixture was inserted in the reactor and sandwiched between two layers of quartz-wool. The reactor was placed in a PID-regulated oven and a K-type thermocouple was inserted in the packed bed. The tests were carried out by heating the packed bed up to 700 °C (heating rate 5 °C/min) under an air flow (100 Nml/min) delivered via a mass flow meter (Brooks). The carbon conversion was indirectly monitored with a NDIR analyzer (ABB) measuring the carbon monoxide and dioxide concentration in the outlet gases. The carbon mass balance was always verified within a ±4% error.

The temperature corresponding to the CO_2 peak (T_p) was taken as an index of the activity of each tested catalyst: the lower the T_p value, the more active the catalyst. The runs were in any case repeated three times and the average T_p value was assumed for each catalyst. The maximum deviation between the three T_p values never exceeded 15 °C. In order to fully appreciate the catalytic effect of the perovskites, blank soot combustion runs in the presence of the only inert SiO_2 were also performed.

The activation energy of soot combustion over the prepared catalysts was measured according to the Ozawa method [14] on the grounds of DSC runs carried out in a Perkin-Elmer DSC-Pyris equipment. About 10 mg of a 9:1 by weight catalyst/carbon mixture were analyzed (the same weight of alumina as a reference) during a temperature scan from 50 to 720 °C (heating rates: ϕ = 5, 10, 20, 30 and 50 °C/min). An air flow (100 ml/min) provided the oxygen required for carbon combustion. DSC patterns were processed thus obtaining the onset and the maximum temperatures of the exothermic combustion peak. DSC scans were also performed (in the experimental conditions reported above) on an alumina/carbon mixture, so as to estimate the activation energy of the non-catalysed carbon combustion. Details about the data handling procedure to evaluate the activation energy are provided in [9,14] and not reported here for the sake of briefness. The precision of this determination is ±5%.

2.4. Catalytic trap preparation

Selected catalysts ($La_{0.8}Cr_{0.9}Li_{0.1}O_3$, $La_{0.8}Cr_{0.8}Li_{0.2}O_3$) were deposited by in situ combustion synthesis directly over ceramic wall-flow filters. The filters were dipped in an aqueous solution of the catalyst precursors (same composition as for the preparations of catalyst powders) and then placed into an oven at 600 °C after draining. The aqueous phase impregnating in the channel pore walls or simply adhering to the channel walls in the form of a thin film was rapidly brought to boil, the precursors mixture ignited and the synthesis reaction took place in situ. The supports selected were:

(1) silicon carbide (SiC) trap produced by IBIDEN;
(2) cordierite ($2MgO{\cdot}2Al_2O_3{\cdot}5SiO_2$) trap produced by CORNING.

The geometrical parameters of both traps were: cell structure = 14/200; diameter = 30 mm; length = 6–12 in.; pore diameter of channel walls = 9 μm; porosity of channel walls = ca. 40%.

Both ceramics were found to be chemically compatible with the selected catalyst.

The amount of perovskites deposited was about 5 wt.%, as assessed by gravimetric analysis. As mentioned above, the morphology of the deposited catalyst layer was analyzed by FESEM observation. A foamy structure of the catalyst is indeed a pre-requisite to obtain good catalyst-to-particulate contact conditions and a rather low pressure drop throughout the channel walls.

Finally, catalyst adhesion to the monolith was assessed by a tailored ultrasonic bath test procedure [4].

2.5. Engine bench testing

The developed trap was tested over in a Diesel engine bench (Kubota 1000 cc IDI engine, capable of up to 23.5 hp at 3000 rpm), where the temperature (K-type thermocouples placed at axial positions) and gas composition (Elsag-Bailey: NDIR for NO, CO, CO_2, SO_2; FID for overall HC; paramagnetic for O_2; filtration over PALLFLEX 47 TX 40 HI 20-W filters for diesel particulate) before and after the trap can be controlled and monitored, as well as the evolution of the pressure drop (VIKA pressure transducers) through the trap, as a consequence of soot accumulation therein. A detailed description of the plant was provided by Fino et al. [4]. In line with the pending 2005 EU regulations, all the tests were carried out by using a low-sulphur (<50 ppmw) diesel oil produced by Agip Petroli.

The following standard bench test procedure was adopted:

- the trap was loaded by letting comparatively cold exhaust gases flow through it until about a 120 mbar pressure drop was reached (corresponding to a soot hold-up of about 10 g l^{-1}, a comparable hold-up used in literature [15,16]);
- regeneration was then induced by post-injecting some fuel (10–13 kg/kg of exhaust gases) with a metering pump and by burning it with an oxidizing honeycomb catalyst (OXICAT by Johnson Matthey) placed just upstream the trap.

The time needed for the complete trap regeneration (e.g. combustion of soot hold-up) is an index of catalyst performance

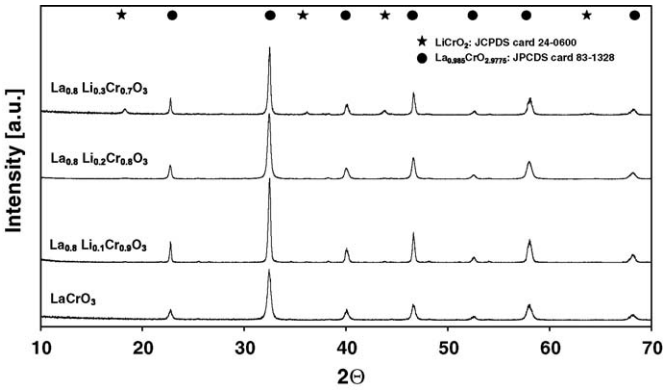

Fig. 1. XRD diffraction pattern of all the catalysts synthesised.

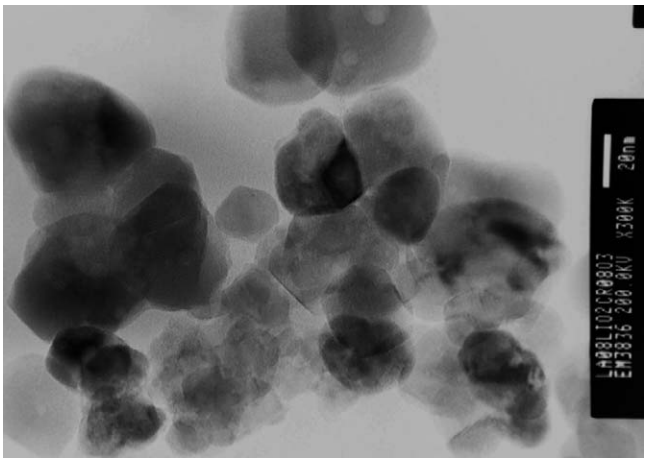

Fig. 2. TEM micrograph of the $La_{0.8}Li_{0.2}Cr_{0.8}O_3$ catalyst crystals.

as well as the completeness of soot combustion. The higher the catalyst activity the lower the required regeneration time. The completeness of the regeneration process was indicated by the decrease of the trap pressure drop till a value practically equal to that measured at the beginning of the loading phase.

Twin runs on virgin, non-catalytic traps were also performed for the sake of comparison.

3. Results and discussion

Atomic absorption analysis (AAS) confirmed that the amount of the various elements of interest (La, Cr, Li) present in the prepared catalysts was consistent with that used in the precursors. Deviations within ±5% for each single element were evaluated, which is in line consistent with the AAS analysis precision.

The diffraction spectra recorded for all the prepared catalysts is shown in Fig. 1: it confirms the presence of a crystalline lanthanum chromite phase (JPCDS card: PDF 83-1328) in any of the catalysts synthesised. However, for the catalyst hosting the highest amount of lithium ($La_{0.8}Cr_{0.7}Li_{0.3}O_3$) some $LiCrO_2$ delafossite (JPCDS card: PDF 24-0600) was also clearly detected as a sign that Li could not completely enter the perovskite structure, at least with the preparation route adopted. Since the detection limit of X-ray diffraction is 4 wt.%, the presence of minor amorphous or crystalline phases cannot be excluded also in the $La_{0.8}Cr_{0.8}Li_{0.2}O_3$ catalyst.

The TEM picture of this last catalyst in Fig. 2 shows however a rather well crystallized sample, which plays in favor of the absence of secondary phases. This picture is indeed representative of the $LaCrO_3$ and $La_{0.8}Cr_{0.9}Li_{0.1}O_3$, as well. Most of the perovskite crystals range between 20 and 50 nm in size, which is in line with the BET specific surface areas (13–17.5 m^2/g) listed in Table 1. The specific surface area exposed by the perovskite crystals is equal to the geometrical one as they do not possess internal microporosity.

Fig. 3 shows the TPC plots obtained for the various catalysts. Conversely, TPC peak temperatures are listed in Table 1 together with the T_p value of non-catalytic combustion (650 °C). As expected, all the catalysts markedly lower the combustion peak temperature compared to that of the non-catalytic combustion.

Compared to the earlier developed $La_{0.8}Cr_{0.9}Li_{0.1}O_3$ perovskite, the compounds related to formulas $La_{0.8}Cr_{0.8}Li_{0.2}O_3$ and $La_{0.8}Cr_{0.7}Li_{0.3}O_3$ are characterized by a higher activity, especially at temperatures lower than 350 °C. These last two catalysts seem to be capable of delivering active oxygen species at lower temperatures than the former counter part. In all cases, Li-containing compounds showed a selectivity towards CO_2 exceeding 96% as opposed to the 87% measured for the reference $LaCrO_3$.

As the increase in Li substitution at the chromium site was thus beneficial for the catalytic activity, further investigations were devoted to understanding the nature of this promotion and the reaction mechanism. Such investigations were though focused exclusively on the $La_{0.8}Cr_{0.8}Li_{0.2}O_3$ in comparison with the catalysts containing lower amounts of Li for two main reasons:

Table 1
Results of catalyst characterization tests concerning catalytic activity, activation energy, BET specific surface area and temperature-programmed desorption of oxygen

Catalyst	BET (m^2/g)	T_p (°C)	E_a (kJ/mol)	Desorbed O_2 in TPD run (μmol/g)	α-type (μmoli/g)	β-type (μmoli/g)
$LaCrO_3$	17.53	495	147.0	23.7	8.0	15.7
$La_{0.8}Li_{0.1}Cr_{0.9}O_3$	12.96	408	135.5	738.7	529.0	209.7
$La_{0.8}Li_{0.2}Cr_{0.8}O_3$	14.12	404	136.7	1221.3	623.2	598.1
$La_{0.8}Li_{0.3}Cr_{0.7}O_3$	16.52	402	–	–	–	–
Non-catalytic combustion	–	650	159.0	–	–	–

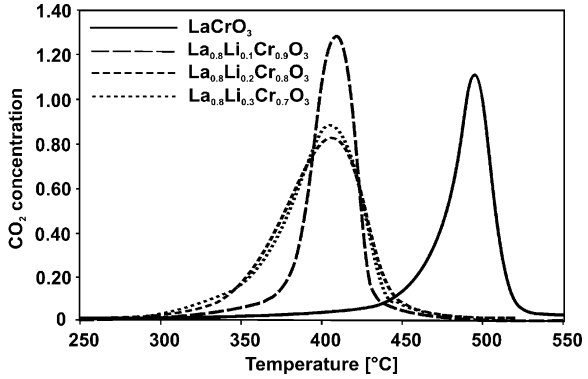

Fig. 3. Results of the TPC runs performed with the perovskite catalysts.

- the activity difference between the $La_{0.8}Cr_{0.8}Li_{0.2}O_3$ and the $La_{0.8}Cr_{0.7}Li_{0.3}O_3$ was not significant;
- $La_{0.8}Cr_{0.7}Li_{0.3}O_3$ turned to be a multiphase compound, which would complicate significantly any mechanistic analysis. It can be anticipated here that deeper investigations are in progress on the role of the $LiCrO_2$ delafossite, which will however be published in future.

As outlined in earlier papers [9,17], the substitution of part of lanthanum with a lower valence alkali metal brings about formation of high valence chromium (Cr^{HV}) to maintain electro-neutrality and possibly to obtain more active or more concentrated oxygen species over the catalyst surface. The activation energies of carbon oxidation over all catalysts, listed in Table 1, are indeed significantly lower than that of non-catalytic combustion. Furthermore, the activation energies for the catalytic reactions are not very different from one another, especially if the experimental error of the Ozawa method (±5%) is considered. This might suggest that all perovskites deliver to the carbon particulates oxygen species of a similar reactivity, which differ, from one sample to another, just for their surface concentration. In line with the speculations in [9] combined TPD/TPR and XPS experiments were carried out to elucidate this point.

Fig. 4 shows the results obtained during oxygen TPD runs. The released oxygen species can be divided into two categories depending on temperature [18]:

- *α oxygen*: low-temperature suprafacial species, weakly chemisorbed on the surface of the perovskite, desorbed in the 300–600 °C range, and related to surface oxygen vacancies;
- *β oxygen*: high-temperature intrafacial one, less easy to desorb and therefore more bound to the perovskite structure, desorbed above 600 °C and related to the bulk nature of the catalyst.

The plots in Fig. 4 show how α oxygen should actually be the primary responsible of the catalytic activity of the various samples.

Table 1 lists the overall amount of oxygen desorbed in the TPD runs, as well as the specific amounts of α and β oxygen species. These data seem to suggest that α- and not β-type oxygen is responsible for the superior activity of Li-substituted chromites towards soot combustion.

The most active single-phase catalyst ($La_{0.8}Cr_{0.8}Li_{0.2}O_3$) is clearly characterized by the highest amount of weakly chemisorbed α oxygen which can possibly undergo *spillover* [2] over the carbon particulates in contact with the catalyst. This should maximize the number of reaction events per unit time and carbon mass thereby boosting reaction kinetics at temperatures even lower than those at which it is desorbed in TPD runs owing to the favorable reaction thermodynamics. In other words, during TPD experiments the only free energy available to oxygen to leave the catalyst is thermal energy. During reaction runs, carbon provides additional free energy to α oxygen and help exploiting it at temperatures lower than those at which it is desorbed during simple TPD runs.

β oxygen, released at higher temperatures, should not play any significant role in soot oxidation. This type of oxygen should indeed dominate the behavior of the various perovskites during TPR runs (Fig. 5). The presence of H_2 was found to induce the release of β oxygen at temperatures lower than those of the TPD case. This anticipation leads to a very sharp and intensive reduction peak, likely lumping both α- and β-species. As opposed to carbon, which can only get in touch with suprafacial oxygen, hydrogen can indeed easily react away also the intrafacial oxygen type, without destroying the perovskite structure in the temperature range of interest, as checked by

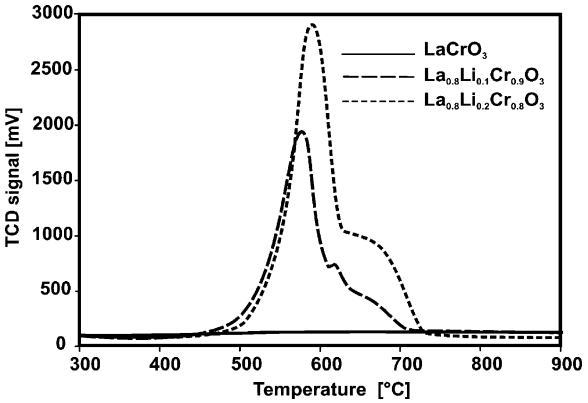

Fig. 4. Temperature-programmed desorption (TPD) plots for the various tested catalysts.

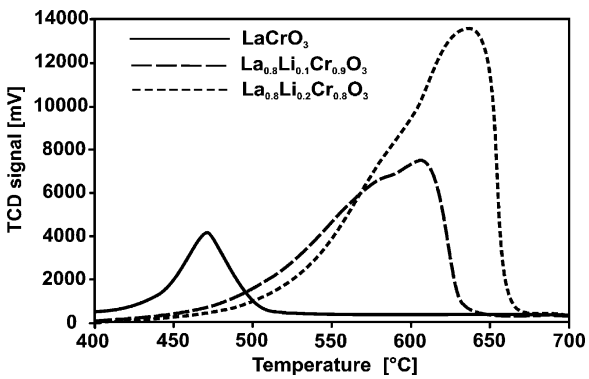

Fig. 5. Temperature-programmed reduction (TPR) plots for the various tested catalysts.

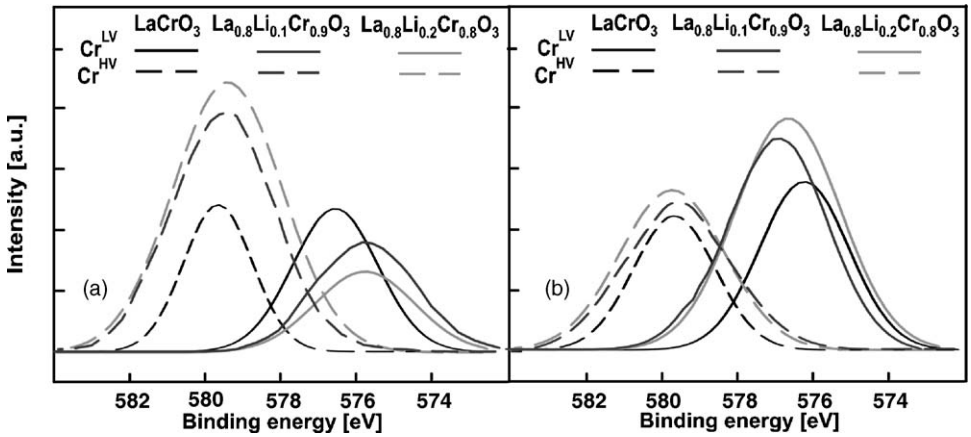

Fig. 6. X-ray photoelectron spectra in the Cr $2p_{3/2}$ region of the perovskite catalysts: (a) after oxidation at 600 °C; (b) after UHV treatment at 400 °C.

XRD. In line with [9], it might be guessed that the presence of the electropositive Li ions in the perovskite structure stabilizes the Cr^{HV} species and renders its bonding to β-type oxygen stronger than that for the basic chromite. The higher this strengthening effect, the more evident the shift towards high temperatures of the TPR peak as compared with that of $LaCrO_3$. However, once again, this feature does not seem to play hardly any role in the combustion of soot for which α-type oxygen should play a prevalent role.

Core level XPS spectra were measured on selected samples after different pre-treatments (oxidation at 600 °C and reduction under UHV at 400 °C) so as to confirm the different nature of the above α and β oxygen species, as well as the valence of the transition metal Cr. The XPS plots for chromium and oxygen are shown in Figs. 6 and 7, respectively. Conversely, Table 2 lists the derived atomic concentrations at the surface of all catalysts tested ($LaCrO_3$, $La_{0.8}Cr_{0.9}Li_{0.1}O_3$, $La_{0.8}Cr_{0.8}Li_{0.2}O_3$).

As for the Cr element, by performing a peak-fitting deconvolution of the overall photoelectron Cr $2p_{3/2}$ peak of the three catalysts after both the oxidation and reduction thermal treatments, the chromium spectrum could be separated into two peaks: the low-valence Cr^{LV} occurring at about 576 eV and the high valence Cr^{HV} characterized by an average binding energy of about 579 eV. The first peak is unequivocally assigned to Cr^{3+} in line with [19]. The second peak defined as ''high valence'', should be assigned to a higher valence chromium state, perhaps Cr^{5+} or Cr^{6+}. XPS data for the latter species are reported to lie in the range 578.0–578.8 eV for Cr^{5+} in $LaCrO_4$ [20] and from 579 to 580 eV for compounds containing Cr^{6+} [21].

As for oxygen, the O 1s spectra could also be de-convoluted into two peaks: one related to lattice β-oxygen type (O^{2-}) with lower binding energy, one related to a binding energy of approximately 531 eV to be attributed to α-oxygen (O^-) weakly bound on the catalyst surface.

As already pointed out in [9], the surface composition of the unsubsituted $LaCrO_3$ perovskite remained practically unchanged after the oxidation and UHV reduction treatment. Conversely, the Li-containing compounds sample got remarkably enriched in Cr^{HV} and O^- species after oxidation. The higher the amount of Li the more intensive the enrichment. After exposure to high vacuum conditions, the ratios Cr^{HV}/Cr and O^-/O decrease dramatically (see also Table 2). It is thus confirmed that the catalytic activity towards carbon combustion of the lithium-substituted chromites, and of the most active

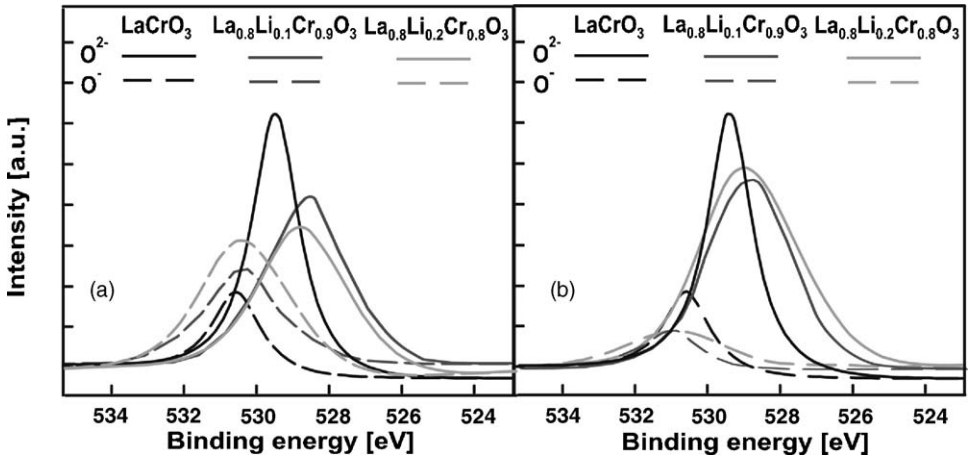

Fig. 7. X-ray photoelectron spectra in the O 1s region of the perovskite catalysts: (a) after oxidation at 600 °C; (b) after UHV treatment at 400 °C.

Table 2
Atomic percent concentrations of La, Cr and O species as derived from XPS analysis on the catalyst samples after specific treatments

Catalyst	Atomic concentrations (%)								
	La	Cr	O	O^{2-}	O^{-}	Cr^{HV}	Cr^{LV}	O^{-}/O	Cr^{HV}/Cr
Samples oxidized at 600 °C in air									
$LaCrO_3$	25.3	14.0	60.7	45.1	15.6	4.8	9.2	0.25	0.30
$La_{0.8}Li_{0.1}Cr_{0.9}O_3$	19.0	18.9	62.1	38.5	23.6	10.4	8.5	0.37	0.55
$La_{0.8}Li_{0.2}Cr_{0.8}O_3$	14.0	19.1	66.9	35.9	31.0	12.5	6.6	0.46	0.65
Samples UHV treated at 400 °C									
$LaCrO_3$	25.8	14.0	60.2	45.6	14.6	4.4	9.6	0.23	0.29
$La_{0.8}Li_{0.1}Cr_{0.9}O_3$	19.5	18.7	61.8	51.8	10.0	5.1	13.6	0.16	0.26
$La_{0.8}Li_{0.2}Cr_{0.8}O_3$	13.1	19.2	65.7	56.6	9.1	5.4	14.1	0.14	0.28

$La_{0.8}Cr_{0.8}Li_{0.2}O_3$ in particular, can be ascribed to their α-oxygen surface storage capacity. The surface oxygen content was found in excess compared to stoichiometry only for the $La_{0.8}Cr_{0.9}Li_{0.1}O_3$ and the $La_{0.8}Cr_{0.8}Li_{0.2}O_3$ compounds, which is perfectly in line with the large amount of α oxygen desorbed by this material during TPD. Furthermore, the α-oxygen storage capacity is strictly related to the presence of Cr^{HV}, a sign of the prevalent role of the redox Cr cycles on the catalytic activity. As a consequence, the La surface concentration decreases despite it does not change at bulk level, in any of studied catalysts hosting lithium.

The most active catalysts ($La_{0.8}Cr_{0.9}Li_{0.1}O_3$ and $La_{0.8}Cr_{0.8}Li_{0.2}O_3$) were lined over the walls of the inlet channels of wall-flow traps of different nature (SiC and cordierite) so as to check the effect of their soot combustion promotion on trap regeneration under practical operating conditions. As catalyst-soot contact is expected to be a crucial issue in this context, the tailored in situ combustion synthesis was adopted to obtain a spongy, though well adhered, catalyst layer. Fig. 8 shows, as an example, the FESEM view of the $La_{0.8}Cr_{0.8}Li_{0.2}O_3$ layer deposited over a cordierite channel wall. Similar results were obtained over the other support (SiC) and with the other catalyst.

The foamy microstructure of the catalyst layer is a consequence of the sudden release of a large amount of gases during the decomposition/combustion of the reacting precursors. Such a microstructure fosters the formation of highly corrugated interfaces, which are expected to intensify the contact between the catalyst and the soot. In the present context, perovskite crystals having a size of the same order of magnitude of that of the particulate (100 nm on average for the last generation of Common Rail Engines [22]) are expected to provide the highest specific number of contact points between these two counter parts.

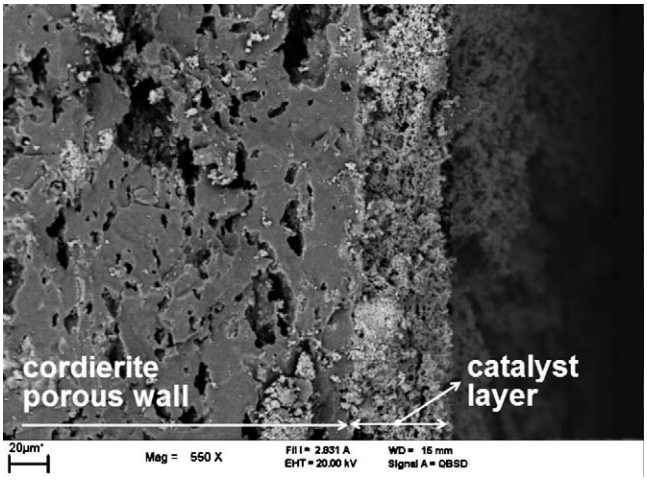

Fig. 8. FESEM view of the microstructure of a $La_{0.8}Li_{0.2}Cr_{0.8}O_3$ catalyst layer deposited over a cordierite wall-flow trap (CORNING).

A second benefit of a spongy catalyst layer lies in the limited pressure drop rise it entails (about 5% higher). Moreover, on the grounds of standardised vibration tests, the adhesion of the deposited catalytic layer was found to be rather good (catalyst loss lower than 0.8 wt.% after tests representative of an entire operating lifetime of a trap [4]).

Coming to the analysis of the developed trap systems performance, Fig. 9 compares the results of the loading and regeneration runs performed with the $La_{0.8}Cr_{0.9}Li_{0.1}O_3$- and $La_{0.8}Cr_{0.8}Li_{0.2}O_3$-catalysed and the non-catalytic cordierite wall-flow monolith. Analogous results are presented for the alternative silicon carbide support in Fig. 10.

A striking difference can be noticed for the two virgin traps. Despite a rather high fuel post-injection is operated (0.13 kg/kg of exhaust gases), leading to inlet trap temperatures well exceeding 600 °C the cordierite trap does not achieve regeneration as opposed to the SiC one. The reason for this is probably related to some slightly different properties of the two different substrates (thermal conductivity, surface roughness of the channel walls, different pore size, uneven soot distribution entailed by the two different systems, etc.). Regeneration is indeed a very complex and activated phenomenon which depends on a number of variables and, once initiated, takes advantage of the heat released by the burning soot to emphasize combustion kinetics. With just a little increase of the post-injection rate (0.14 kg/kg of exhaust gases) the cordierite support could effectively be regenerated.

This scenario is significantly influenced by the presence of the catalysts. All catalysts could in fact induce trap regeneration for both supports and with a lower fuel post-injection rate (0.10 kg of fuel per kg of exhaust gases) sufficient to increase the inlet trap temperature to just 550 °C. Furthermore, regeneration is faster and more complete than for the non-catalytic traps. It is very likely that the catalytic reaction starts

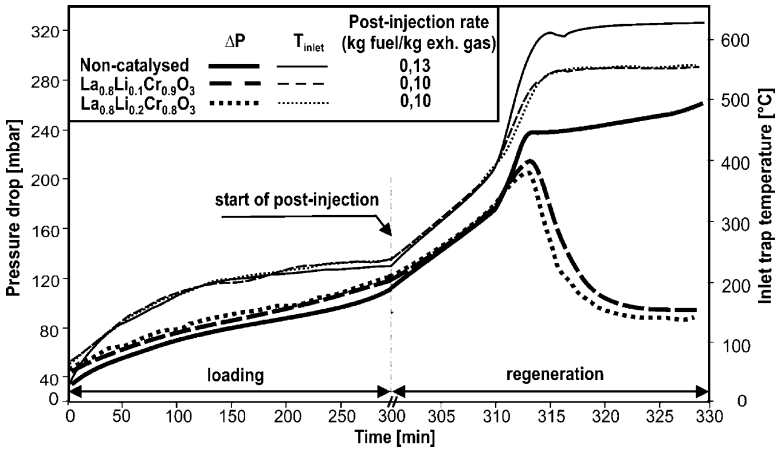

Fig. 9. Loading and regeneration cycle for the non-catalytic (a) and the catalytic ($La_{0.9}Li_{0.1}Cr_{0.9}O_3$, $La_{0.8}Li_{0.2}Cr_{0.8}O_3$) (b) wall-flow cordierite traps; superficial gas velocity = 0.205 m/s.

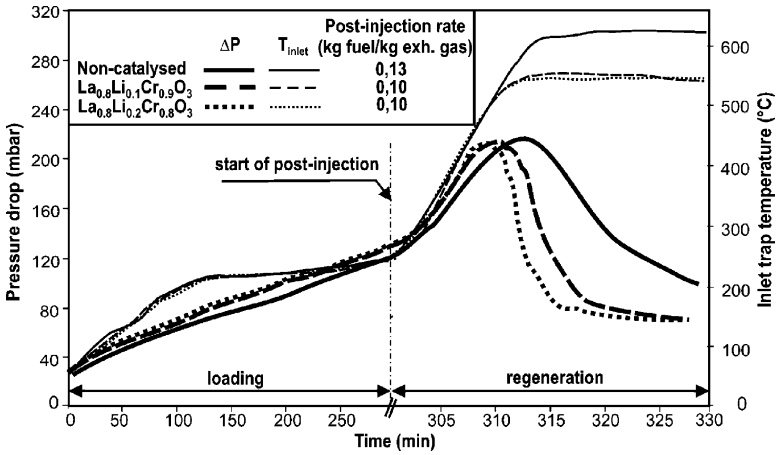

Fig. 10. Loading and regeneration cycle for the non-catalytic (a) and the catalytic ($La_{0.9}Li_{0.1}Cr_{0.9}O_3$, $La_{0.8}Li_{0.2}Cr_{0.8}O_3$) (b) wall-flow SiC traps; superficial gas velocity = 0.205 m/s.

operating even below 400 °C during the post-injection phase. However, to achieve a rapid and complete regeneration 550 °C need to be approached. Under these operating conditions it is likely that portions of soot might get burned by non-catalytic direct oxidation with oxygen owing to some localised overheating. The role of the catalyst remains though essential either to initiate and support soot combustion or to lead regeneration to a higher degree of completeness. It is likely that both α and β oxygen types delivered by the catalyst play a role in the regeneration process, the former during the temperature rise period, the latter when 550 °C are reached.

The more active the catalyst the better the results: the $La_{0.8}Cr_{0.8}Li_{0.2}O_3$-catalysed trap get regenerated faster than those hosting the $La_{0.8}Cr_{0.9}Li_{0.1}O_3$ catalyst. The former catalyst induced a two-fold faster regeneration than that occurring with the non-catalytic SiC trap, despite the lower amount of post-injected fuel. This should directly allow to halving the fuel penalty related to post-injection. Furthermore, the regeneration completeness (77%, determined by trap weighing before and after regeneration) as markedly higher than that of the non-catalytic SiC trap (54%) which should entail a prolongation of the time interval between two subsequent regenerations thereby further reducing the operating costs.

However, it has to be kept into account that the part of fuel savings are compensated by the slight decrease of filter permeability induced by the presence of the catalyst and the related back-pressure.

Finally, in order to fully assess the potential of the prepared traps, their performance should be checked under different engine operating points and especially after prolonged operation, which is planned for the near future.

4. Conclusions

Several Li-substituted chromite catalysts ($La_{0.8}Cr_{0.9}Li_{0.1}O_3$, $La_{0.8}Cr_{0.8}Li_{0.2}O_3$, $La_{0.8}Cr_{0.7}Li_{0.3}O_3$) were prepared by combustion synthesis, characterized and tested as catalysts for soot combustion. The $La_{0.8}Cr_{0.8}Li_{0.2}O_3$ perovskite exhibits the highest activity (even below 350 °C) as a consequence of its superior amount of weakly chemisorbed O^- species (α-oxygen) that were pointed out as the key players in the soot

oxidation. The $La_{0.8}Cr_{0.7}Li_{0.3}O_3$ sample was found to be as active as the above catalyst but it turned to be not well crystallized owing to the non-negligible presence of the $LiCrO_2$ delafossite, a sign that the La-substoichimetric $L_{0.8}CrO_3$ might likely not host such high Li content.

In a subsequent effort, the best catalysts ($La_{0.8}Cr_{0.9}Li_{0.1}O_3$, $La_{0.8}Cr_{0.8}Li_{0.2}O_3$) were lined over cordierite and SiC wall-flow monolith traps and tested according to a standard loading and regeneration cycle. The $La_{0.8}Cr_{0.8}Li_{0.2}O_3$ in particular was found to allow a more complete regeneration of the non-catalytic traps in at least two-fold shorter time and with a lower post-injected fuel flow rate. An experimental test campaign is currently in progress to verify this potential under different engine operating conditions and after repeated regeneration cycles (prolonged operation). Moreover, any possible loss of toxic chromium species will be ascertained at this level.

References

[1] J.P.A. Neeft, M. Makkee, J.A. Moulijn, Diesel particulate emission control, Fuel Process. Technol. 47 (1996) 1.

[2] B.A.A.L. van Setten, M. Makkee, J.A. Moulijn, Science and technology of catalytic diesel particulate filters, Catal. Rev.: Sci. Eng. 43 (2001) 489.

[3] S.J. Jelles, M. Makkee, J.A. Moulijn, G.K. Acres, J.D. Peter-Hoblyn, Diesel particulate control. Application of an activated particulate trap in combination with fuel additives at an ultra low dose rate, SAE Technical Paper Series 1999-01-0113, Society of Automotive Engineers, Detroit, 1999.

[4] D. Fino, P. Fino, G. Saracco, V. Specchia, Innovative means for the catalytic regeneration of particulate traps for diesel exhaust cleaning, Chem. Eng. Sci. 58 (2003) 951.

[5] D. Fino, V. Specchia, Compositional and structural optimal design of a nanostructured diesel-soot combustion catalyst for a fast-regenerating trap, Chem. Eng. Sci. 59 (2004) 4825.

[6] P. Ciambelli, V. Palma, P. Russo, S. Vaccaro, Performances of a catalytic foam for soot abatement, Catal. Today 75 (2002) 471.

[7] P. Ciambelli, P. Corbo, V. Palma, P. Russo, S. Vaccaro, B. Vaglieco, Study of catalytic filters for soot particulate removal from exhaust gases, Top. Catal. 15/16 (2001) 279.

[8] A.G. Konstandopoulos, M. Kostoglou, E. Skaperdas, E. Papaioannou, D. Zarvalis, E. Kladopoulou, Fundamental studies of diesel particulate filters: transient loading, regeneration and aging, SAE Paper Number 2000-01-1016, pp. 189–211 in SAE volume SP-1497 "Diesel Aftertreatment 2000", edited by the Society of Automotive Engineers, Detroit, 2000.

[9] N. Russo, D. Fino, G. Saracco, V. Specchia, Studies on the redox properties of chromite perovskite catalysts for soot combustion, J. Catal. 229 (2005) 459.

[10] A. Civera, M. Pavese, G. Saracco, V. Specchia, Combustion synthesis of perovskite-type catalysts for natural gas combustion, Catal. Today 83 (2003) 199.

[11] D.A. Shirley, High-resolution X-ray photoemission spectrum of the valence bands of gold, Phys. Rev. B 5 (1972) 4709.

[12] J.H. Scofield, Hartree-Slater subshell photoionization cross-sections at 1254 and 1487 eV, J. Electron Spectr. Rel. Phen. 8 (1976) 129.

[13] D. Fino, G. Saracco, V. Specchia, Filtration and catalytic abatement of diesel particulate from stationary sources, Chem. Eng. Sci. 57 (2002) 4955.

[14] T. Ozawa, Critical investigation of methods for kinetic analysis of thermo-analytical data, J. Thermal Anal. 7 (1975) 601.

[15] A. Mayr, J. Klement, M. Ranalli, S. Schmidt, Diesel fuel vaporizer: a way to Reliable DPF Regeneration, SAE Technical Paper Series, SAE_NA 2003-01-50.

[16] M. Masoudi, Pressure drop of segmented diesel particulate filters, SAE Technical Paper Series, SAE 2005-01-0971.

[17] G. Saracco, G. Scibilia, A. Iannibello, G. Baldi, Methane combustion on Mg-doped $LaCrO_3$ perovskite catalysts, Appl. Catal. B 8 (1996) 229.

[18] T. Seyama, Total oxidation of hydrocarbon on perovskite oxides, Catal. Rev.: Sci. Eng. 34 (1992) 281.

[19] W.Y. Howng, R.J. Thorn, Investigation of the electronic structure of La/sub 1 − *x*/(M/sup 2+/)/sub x/CrO/sub 2/, Cr/sub 2/O/sub 3/ and La/sub 2/O/sub 3/ by X-ray photoelectron spectroscopy, J. Chem. Phys. Solids 41 (1980) 75.

[20] H. Konno, H. Tachikawa, A. Furusaki, R. Furuichi, Characterization of lanthanum(III) chromium(V) tetraoxide by X-ray photoelectron spectroscopy, Anal. Sci. 8 (1992) 641.

[21] G.C. Allen, P.M. Tucker, Multiplet splitting of X-ray photoelectron lines of chromium complexes—effect of covalency on 2*p* core level spin-orbit separation, Inorg. Chim. Acta 16 (1976) 41.

[22] M. Ambrogio, G. Saracco, V. Specchia, C. van Gulijk, M. Makkee, J.A. Moulijn, On the generation of aerosol for diesel particulate filtration studies, Sep. Purif. Technol. 27 (2002) 195.